Title: Electrochemical aging and characterization of graphite-polymer based composite bipolar plates for vanadium redox flow batteries

Gaurav Gupta[a], Barbara Satola[a], Lidiya Komsiyska[a, #], Corinna Harms[b], Thorsten Hickmann[c] and Alexander Dyck[a]

[a]German Aerospace Center, Institute of Networked Energy Systems, Carl-von-Ossietzky-Str. 15, 26129 Oldenburg, Germany

[b]German Aerospace Center, Institute of Engineering Thermodynamics, Carl-von-Ossietzky-Str. 15, 26129 Oldenburg, Germany

[c]Eisenhuth GmbH & Co. KG, Friedrich-Ebert-Str. 203, 37520 Osterode, Germany

Corresponding Author E-mail Address: Corinna.Harms@dlr.de

[#]Present address: Technische Hochschule Ingolstadt, Esplanade 10, 85049 Ingolstadt, Germany

Abstract Text

Three bipolar plates (BPP) comprised of a composite of polypropylene or polyvinylidene fluoride polymer and varying average graphite particle size were studied for application in a vanadium redox flow battery (VRFB). The BPPs were electrochemically aged via 3000 cyclic voltammetry curves in 1.8 M $VOSO_4$ + 2.0 M H_2SO_4 electrolyte. After every 500th cycle the aging progression was determined by performing cyclic voltammetry on the bipolar plates in 0.1 M H_2SO_4 solution where the double layer capacitance, the quinone/hydroquinone and the vanadium species redox activity were quantitatively evaluated. Prior to the aging, the composite plates were extensively characterized using various physical methods. The performed studies reveal that the wettability, surface roughness and accessible porosity of the bipolar plates significantly influence their electrochemical stability. Cycling tests in vanadium redox flow single cells at a constant current density of 60 mA cm^{-2} revealed a close correlation of the cell efficiencies to the electrochemical stability of the bipolar plates. Thus, the proposed electrochemical characterization method can be an effective foresight to

predict the applicability of a bipolar plate in a vanadium redox flow battery.

Introduction

The world is transitioning from non-renewable to renewable energy sources such as wind and solar power. These sources are environmentally friendly and cost efficient, however, their inability to generate power constantly hinders their adaptability (1). This issue can be overcome by deployment of energy storage systems such as redox flow batteries (RFBs). The significant advantage of RFBs is their ability to scale the power and energy capacity independently, i.e. higher power can be achieved by increasing the electrode area or number of cells in series while higher electrolyte volume or molar concentrations would raise the capacity (2-4). Moreover, as the electrolytes are water-based, fire hazard is reduced compared to lithium-ion battery systems (5).

The all vanadium redox flow battery (VRFB) owed to its high cycling life, quick response time (4) and deep-discharge capability (6) has attracted a lot of attention for grid-scale energy storage system (3) and provides power at peak time (7). As vanadium is the redox couple in both half-cells, rebalancing of the electrolyte can restore the capacity loss caused by vanadium species crossover (2, 3). The VRFB stack consists of porous electrodes, bipolar plates (BPP), membranes and current collectors(4, 8). The positive (VO_2^+/VO^{2+}) and negative (V^{2+}/V^{3+}) electrolytes are composed of dissolved vanadium ions in a sulfuric acidic solution and stored in separate reservoirs. The electrolytes are pumped through each half-cell during battery operation and the half-cells are separated by an ion exchange membrane (8, 9). The electrochemical reactions occur on the surface of the porous electrodes as shown below

Positive electrode: $VO_2^+ + 2H^+ + e^- \leftrightarrow VO^{2+} + H_2O$ $E° = + 1.0$ V vs. SHE

Negative electrode: $V^{2+} \leftrightarrow V^{3+} + e^-$ $E° = - 0.26$ V vs. SHE

Overall reaction: $VO_2^+ + V^{2+} + 2H^+ \leftrightarrow VO^{2+} + V^{3+} + H_2O$ $U° = + 1.26$ V vs. SHE

The BPPs conduct electrical current and substantially influence the power capability of the VRFB, while separating electrolyte solutions between the adjacent cells and also providing mechanical integrity to the VRFB stack (4). Hence, it is essential that the BPPs have high mechanical strength, low ion permeability, high electrical conductivity and low contact resistance to the porous electrode. Apart from these, for application in a VRFB other desired characteristics of a BPP is their chemical and electrochemical stability (4, 9) and high

overpotential to hydrogen and oxygen evolution (9).

BPPs can be generally divided into three categories: metallic, graphitic and composite type (4, 8). The high electrical conductivity and easy formability make the metallic BPPs quite attractive (8), but low stability in an acidic medium impedes their use in VRFBs (4, 8, 9). The graphitic BPPs have high chemical stability accompanied with good electrical conductivity [4], however, their poor processability, low mechanical strength, high cost (4, 8, 9) and porous structure (9) make them unattractive for the application in RFBs. The composite BPPs owed to their high chemical stability, mechanical strength, low production cost (4, 6) and light weight (6) are a viable option. The polymer, such as thermoplastics (e.g. polyethylene) and thermosets (4, 9), provide the matrix for the mechanical integrity and carbon-based fillers like graphite, carbon black and carbon nanotubes (4, 9) impart the conductive properties. It has been reported that the type (6, 7) and particle size (8, 10) of graphite can have a significant effect on the electrical and electrochemical properties of the BPP.

Even though the vanadium redox reactions as well as side reactions, such as oxygen and hydrogen evolution, occur on the graphite felt electrodes during battery operation, some working groups (4, 9, 10) have reported that occasionally electrochemical reactions may also occur on the BPP surface. This can happen if an abnormal current passes through the VRFB electrolyte causing the sulfuric acid in the electrolyte to oxidize the BPP. This phenomenon may affect the integrity of the BPP and negatively influence the VRFBs performance (7).

A few studies have been published describing various electrochemical characterization methods and VRFB cycling tests. Cyclic voltammetry (CV) on a carbon-polythene composite BPP was performed in a 2 M $VOSO_4$ + 2 M H_2SO_4 at 20 °C by potentiodynamic polarization from 0 to 2.5 V vs. SCE at a scan rate of 5 mV s^{-1} (6). It was demonstrated that the carbon-polythene composite BPP had higher gas evolution potentials and better electrochemical stability compared to a graphite felt and a graphite electrode. Despite the suppression of gas evolution, the new BPP showed severe structural erosion and decline in electrical conductivity. In another study, a graphite-polymer composite BPP consisting of large flake type major filler with 80 µm and minor filler with 50 nm, was characterized electrochemically in a 0.1 M $VOSO_4$ + 3 M H_2SO_4 electrolyte solution. The CV measurement was performed by sweeping between -0.2 and +1.6 V vs. Ag/AgCl at a scan rate of 5 mV s^{-1}

(8). The developed composite BPP showed suppressed oxygen evolution. Single cell VRFB tests with the developed and commercial BPPs at current densities of 40, 60, 80, 100 mA cm^{-2} were also performed. The new BPP exhibited an energy efficiency decay of 0.87% compared to 2.5% for the commercial one. While Zhang et al. a carbon-polypropylene thermoplastic elastomer (PP-elastomer) composite BPP was compared to a graphite BPP in a 1.5 M $VOSO_4$ + 2.0 M H_2SO_4, here CV was performed by sweeping between -0.1 and +2.0 V vs. SCE at a scan rate of 20 mV s^{-1} (10). The CV of the graphite BPP showed significant vanadium redox activity ($VO^{2+} \rightleftarrows VO_2^+$ and $V^{3+} \rightleftarrows V^{2+}$). In contrast, the PP-elastomer composite BPP exhibited only a cathodic peak ($VO_2^+ \rightarrow VO^{2+}$). Furthermore, a 5-cell VRFB stack test at a current density of 50 mA cm^{-2} with the prepared PP-elastomer composite BPP achieved a stable performance for 2300 cycles with an average energy efficiency of 75% while the graphite BPP broke down after 1450 cycles and the test was discontinued. In another investigation by Lee et al. carbon polymer (epoxy resin) composite BPP (15 wt% carbon black) was prepared and characterized by comparing it against a conventional BPP by potentiodynamic cycling in 2.5 M H_2SO_4 by sweeping from +0.1 to +2.0 V vs. SCE at a scan rate of 5 mV s^{-1} (11). The composite BPP exhibited lower corrosion current densities compared to the conventional BPP. Though, single cell VRFB test at current density of 40 mA cm^{-2} revealed similar energy efficiencies for both BPPs.

Apart from the reported potentiodynamic methods, galvanodynamic characterization has also been reported (12). A graphite-polypropylene composite BPP was galvanodynamically aged in a positive vanadium electrolyte with 1.6 M VO_2^+/VO^{2+} + 2 M H_2SO_4 + 0.05 M H_3PO_4at varying states of charge (10, 50 and 90%). The CV was recorded by sweeping the current density between +100 mA cm^{-2} and -100 mA cm^{-2} at a scan rate of 20 mA s^{-1}. The aged BPPs were examined in a diluted H_2SO_4 solution to assess the effect of aging by sweeping between 0 V and +1.05 V vs. Hg/Hg_2SO_4 at a scan rate of 5 mV s^{-1}. Here, three aging indicators, the double layer capacitance (C_{dl}), the quinone/hydroquinone ($Q_{Q/HQ}$) and the vanadium redox activity ($Q_V{}^{4+}{}_{/V}{}^{5+}$) were identified. They evaluated these aging indicators and related them to increased hydrophilicity of the BPP and oxidation of the graphite compound (12).

From above it can be derived that the constituents, the graphite particle size and wt.% composition can significantly affect the electrochemical behaviour of a BPP (6, 8, 10, 11).

Furthermore, surficial properties of a BPP such as hydrophilicity and surface roughness could be an indication of their electrochemical stability (12). In the current contribution three different graphite-polymer composite BPPs were subjected to identical electrochemical characterization and compared to single cell VRFB tests in order to determine if preliminary electrochemical investigations might forecast the performance of BPPs in real battery application. The work correlates the influence of surficial properties to the electrochemical behaviour and to the VRFB efficiencies.

Experimental

In this study three types of compress molded graphite-polymer composite BPPs (Eisenhuth GmbH & Co. KG, Germany) were investigated (Table 1). The studied composite BPPs constitute either polypropylene (PP) or polyvinylidene fluoride (PVDF) polymers and different graphite types with small graphite (GS) or large graphite (GL) particles sizes (PS).

As a pre-treatment all as received BPPs were cleaned with ethanol solution and dried with low coarse tissue paper (Kimtech, USA). These BPPs are referred as pristine.

In order to study the structural and physical morphology of GS and GL particles the two raw graphite powders were imaged and their average graphite PS was quantified using X-ray computed micro tomography (mCT, SkyScan 1172, Bruker, Belgium). For the mCT scan the raw graphite powders were introduced on to the sample holder which was then placed onto the measuring stage. The scan resolution was set to 1 µm/pixel with a source voltage of 80 kV, rotation step of 0.18° and rotation angle from 0° to 180°. Averages of six frames were recorded to generate a set of cross-sections of images in gray scale. The recorded gray scale data was loaded onto the NRecon software (SkyScan, Bruker, Belgium) where the 3D images were reconstructed. The range of the histogram from the gray scale, value of ring artefact reduction and beam hardening were kept the same for each graphite powder. A volume of interest (VOI) of 2000 µm x 2000 µm x 1000 µm was defined for quantification of the PS size (CTAn, SkyScan, Bruker, Belgium). A series of operations were defined for analysis in the following order (i) filtering and despeckling was done to eliminate the background noise, (ii) binary imaging was performed by bitmap operation through qualitative determination of the minimum and maximum values on the threshold scale to segment the image between

graphite particles (white) and background (black) followed by (iii) morphological and quantitative 3D analysis to determine the average graphite PS.

The accessible porosity was determined through intrusion of mercury into the accessible pores of the BPPs. The BPPs were introduced into a dilatometer and placed onto a mercury porosimetry device (Pascal 140, Pascal 400, Thermo Fisher Scientific S.p.A., Italy). The accessible porosity percentage was estimated using SOL.I.D. software (Thermo Fisher Scientific S.p.A., Italy).

The density of each BPP was defined by measuring the mass on a lab weighing scale and dividing it with the volume.

$$D = M/V$$

Where, {D: density [g cm^{-3}], M: mass[g] and V: Volume[cm^{-3}]}

In-plane electrical resistivity was measured on a four-point probe testing unit (RM3-AR, Jandel, UK) (Figure 1 (a)). Five measurements were performed on different locations of each BPP surface and the average electrical conductivity (σ_{in}) was calculated. The through-plane electrical conductivity of the BPP was measured on an adapted strain/compression testing machine (ZwickRoell, Ulm, Germany) (Figure 1 (b)). The BPP was placed between two gold plated copper stamps. In order to improve the contact between the BPP and stamp surfaces and for better comparison between samples with different surface topology, gas diffusion layer sheets (GDL, Freudenberg Group, Germany) were placed in between. The current was applied, and voltage drop was measured on a multimeter (Tektronix Corporation, DMM 4050, USA). A constant pressure of 1 N mm^{-2} was applied. Usually, after roughly 1 min the resistance value was stable and it was noted after 3 min. Three measurements were done per BPP and the average through-plane electrical conductivity (σ_{th}) was calculated.

$$\sigma_{in=} 1/p \qquad \sigma_{th} = L/RA$$

Where σ_{in} : in – plane electrical conductivity [S cm^{-1}]

σ_{th} : through – plane electrical conductivity [S cm^{-1}]

L : thickness of BPP [cm], R: resistance [Ω], A : area of BPP[cm^2], p; resistivity

The aging and analysis of the BPPs was done in two separate three-electrode setups, each consisting of the investigated BPP as working electrode (WE), Ag/AgCl in 3 M KCl (+0.210

V vs. SHE) as reference electrode and the counter electrode was a platinum mesh attached to a thermally treated porous graphite felt (GFD4.6EA, SGL Carbon group, Germany). The test setups were placed in a Faraday cage. The potential sweeps were applied by a potentiostat/galvanostat (VersaSTAT 3F, Ametek, USA). The BPP was placed in a sample holder (Metrohm Autolab B. V., Netherlands) made of PP and sealed with a polytetrafluoroethylene seal locking ring. The active area of the BPP was 1 cm^2. Prior to each measurement the aging and analysis solutions were purged with nitrogen gas for at least 15 minutes and during the measurement nitrogen gas was maintained in the gas compartment above the liquid phase in the three-electrode setup. The electrochemical aging and analysis routine was performed as follows.

(i) Pre-aging: CV was performed by cycling the pristine BPP in 0.1 M H_2SO_4 solution between +1 and -0.2 V vs Ag/AgCl at a scan rate of 5 mV s^{-1}. Two CV cycles were performed per BPP. The second cycle was evaluated.

(ii) Electrochemical aging: The CV were performed by cycling the BPP in 1.8 M $VOSO_4$ + 2 M H_2SO_4 electrolyte solution between +1.7 and +0.7 V vs. Ag/AgCl at a scan rate of 200 mV s^{-1}. A total of 3000 CVs were performed. After every 500th aging cycle post-aging (iii) analysis was performed.

(iii) Post-aging: After every 500th aging cycle the BPP was removed from the vanadium electrolyte, rinsed and immersed in millipore water after which the BPP was dried carefully using compressed air and low coarse paper. The post-aging analysis was done in 0.1 M H_2SO_4 solution with the same test conditions as for the pre-aging analysis. For every trial a fresh 0.1 M H_2SO_4 solution and thermally treated porous graphite felt for the counter electrode was used. Two CV cycles were performed per BPP. The second cycle was evaluated to determine the aging progression.

The quantitative evaluation of the post-aging CVs was performed on the basis of $C_{dl,}$, $Q_{Q/HQ}$ and $Q_V{}^{4+}{}_{/V}{}^{5+}$ of vanadium ion traces (Figure 2). For the electrochemical characterization measurement three trials were done per BPP.

For C_{dl} the anodic and cathodic current density was selected at points where no redox activity was observed (dashed line in Figure 2(a)). $Q_{Q/HQ}$ was calculated in the range between +0.2 to +0.4 V vs. Ag/AgCl (Figure 2(a)) and as reported (12, 13) $Q_V{}^{4+}{}_{/V}{}^{5+}$ was calculated in the

range between +0.7 to +0.9 V vs. Ag/AgCl (Figure 2(a)). For the integration and evaluation of $Q_{Q/HQ}$, $Q_V^{4+}{}_{/V}^{5+}$ the respective, C_{dl} was subtracted.

The static surface wettability of BPPs was measured with contact angle system OCA 15plus (Data physics, Germany). The device was equipped with a Hamilton 500 µL syringe, a charge-couple device camera and a SCA20 software (version 2.0.0, Data physics, Germany). Using the sessile drop method 4 µL of deionized water was introduced onto the surface of the BPP and the contact angle was measured. Six measurements were done for each BPP to determine the average value.

The BPP's surface roughness was measured using a confocal microscope (Sensofar, PLu neox, Spain). The microscope was set to 100x magnification and on the SensoScan software (Sensofar, PLu neox, Spain) a vertical step size of 32 µm was used to measure an area of 127.32 µm x 95.45 µm. The root mean square surface roughness (S_q) was calculated and five measurements were done for each BPP to estimate the average S_q.

A single flow cell (CNL Energy co, Republic of Korea) was assembled for galvanostatic charge and discharge tests. Thermally treated (in air at 400 °C, 18 h) XF30A carbon felts (4 mm, Toyobo, Japan) with an active area of 5 cm x 5 cm were used as electrodes. The half-cell was separated by Nafion 117 (DuPont, USA) cation-conducting membrane (pre-treated in 10% H_2O_2 solution, 80 °C, 30 min). The polymer-graphite composite BPP(s) were placed between the carbon felt electrode and the gold coated nickel current collector. The cell was operated at a constant current density of 60 mA cm^{-2} which was applied through a potentiostat/galvanostat (VersaSTAT 4, Ametek, USA). The electrolyte 1.8 M $VOSO_4$ in 2 M H_2SO_4 was prepared by dissolving anhydrous $VOSO_4xH_2O$ (Sigma-Aldrich, USA) in diluted H_2SO_4 (Sigma-Aldrich, USA). Prior to each single cell test the oxidation state of the electrolyte had to be balanced. This was done by filling the tank of the positive side with 80 ml and of the negative side with 40 ml electrolyte. The electrolytes were pumped through their respective half-cell at a flow rate of 25 ml min^{-1} (KNF, Germany). The cell was charged to +1.7 V. Following the first charging step 40 ml of electrolyte was removed from the positive side and then the cell was discharged with the positive and negative tank each containing 40 ml of electrolyte. After which the single cell test was initiated by performing 200 charge/discharge cycles between +1.7 to +1 V. During the electrolyte balancing and

single cell test the negative electrolyte was continuously purged with nitrogen gas. One trial was done per BPP.

The single cell VRFB tests were evaluated as follows:

Voltage efficiency, $\eta_V = \frac{\int_{t1}^{t2} V_{discharge}(t)dt}{\int_{t1}^{t2} V_{charge}(t)dt}$ [%]

Columbic efficiency, $\eta_{Ah} = \frac{Q_{discharge}}{Q_{charge}} = \frac{\int_{t1}^{t2} I_{discharge}(t)dt}{\int_{t1}^{t2} I_{charge}(t)dt}$ [%]

Energy efficiency, $\eta_{Wh} = \eta_V \times \eta_C$ [%]

State of Health, SoH $= \frac{Q_{discharge}^{N}}{Q_{discharge}^{1st}}$

Where V; voltage [V], I : current [A], Q: charge [C], during charge and discharge cycles t: time [h] and N is the discharge cycle number.

All the above-mentioned measurements were done at room temperature.

Results

As explained in the experimental section three BPPs, named PP-GS, PVDF-GS and PVDF-GL, were studied with each BPP composed of GL or GS. The mCT 2D images of the pure GL and GS powders (Figure 3) revealed that the graphite particles vary in shape, PS and size distribution. The corresponding average graphite PS values are listed in Table 2.

Discussion

The accessible porosity was quantified using mercury porosimetry and confocal microscopy provided S_q of each BPP highlighting the influence of the constituents on the composite material characteristics (Table 2). It can be inferred that the larger graphite PS in PVDF-GL lead to larger or more accessible pores and higher surface roughness probably due to protruding graphite particles on the surface. In comparison, the PVDF-GS and PP-GS BPPs are comprised of smaller graphite particles exhibiting smoother surfaces and lower accessible porosity. Here it should be noted that not only the graphite filler-type/PS, but also the manufacturing process and the used polymer influence the surface properties of the BPPs. However, since the PP based BPP constitutes different filler to polymer ratio to that of the PVDF based BPPs, a direct conclusion on the influence of the PP or PVDF on the surface roughness cannot be drawn in the current contribution. Nevertheless, it is worth mentioning,

that the PP-GS BPP showed rather a smooth and probably homogenous surface.

Another important parameter of the composite materials is their density. In general, the density of PVDF it is 1.65 – 1.97 g cm^{-3} (14) while of graphite is 1.9 – 2.2 g cm^{-3} and of PP it is 0.9 g cm^{-3} (15) .The lower density in conjunction with the lower polymer content of PP in comparison to the other two PVDF BPPs would explain the low-density value for PP-GS (Table 2). Whereas, for the higher density values of PVDF-GS and PVDF-GL the primary influencer is the density of PVDF.

The varied PS of the graphite powders and the selection of polymer types also influence the electrical conductivity behaviour of each BPP. Both PVDF based composite BPPs with 80% graphite content each exhibit higher in- and through-plane electrical conductivities compared to the PP-GS (Figure 4), even though the PP based BPP is composed of higher graphite weight percentage of 86%. It is assumed that the properties of the PVDF, such as higher density, might provide better connected pathways between the conductive graphite particles within the composite structure. Hence, the PVDF-GS and PVDF-GL exhibit higher and comparable electrical conductivity values. The higher standard deviation for PVDF-GL and PVDF-GS is probably due to the higher S_q.

To assess the influence of the surface properties and composite composition of the BPPs on their electrochemical stability, the pristine BPPs were subjected to continuous potential sweeping in high concentrated 1.8 M $VOSO_4$ + 2 M H_2SO_4 electrolyte. The aging progression of the BPPs was monitored via intermittent CV measurements in 0.1 M H_2SO_4 solution. The pre-aged CV curves (Figure 5 (a)) in 0.1 M H_2SO_4 solution of the studied BPPs show that the pristine PVDF-GL has the most discernible C_{dl} and $Q_{Q/HQ}$ features. The C_{dl} is influenced by BPP surface-electrolyte interaction and can be related to surface hydrophilicity and roughness (12, 16). It is probable, that the PVDF-GL exhibits larger graphite-electrolyte interface in good agreement with the highest observed surface roughness. Whereas, the pristine PP-GS with the lowest electrical conductivity and lowest surface roughness values, shows the least current response in terms of C_{dl} . In addition, the $Q_{Q/HQ}$ characteristics of PVDF-GL could be attributed to a higher amount of oxygen functional groups as reported by Satola et al. (12).

Comparing the aging progression for each individual BPP (Figure 5 (b), (c) and (d)), the

expected aging behaviour was observed, i.e. increasing C_{dl} , rising $Q_{Q/HQ}$ activity and presence of vanadium species redox activity Q_V^{4+}/V^{5+} . All features were quantitatively evaluated and plotted (Figure 6). In general, the increasing C_{dl} (Figure 6 (a)) is induced primarily by increased hydrophilicity and high surface area leading to higher BPP surface-electrolyte interaction area (12, 16). Whereas, the $Q_{Q/HQ}$ activity (Figure 6 (b)) is related to the oxidation of the graphite components in the BPPs (4, 12) and is further increasing the hydrophilicity. Moreover, even though prior to post-aging analysis each BPP was cleaned with Millipore water, the accessible porosity of the BPP could have caused entrapment of vanadium species within pores causing vanadium redox activity Q_V^{4+}/V^{5+} (4, 12, 13).

The PVDF-GL exhibits the highest values for C_{dl} , $Q_{Q/HQ}$ and Q_V^{4+}/V^{5+} (Figure 6 (d)). The measured water contact angle and surface roughness for the PVDF-GL (Figure 7) indicate that it had the highest hydrophilicity and surface roughness in pristine state which would lead to significantly higher BPP-electrolyte contact with a progressive increase of electrochemical aging . Whereas, the pristine PVDF-GS and PP-GS have lower hydrophilicity, surface roughness values, and lower accessible porosity which led to reduced electrochemical aging. Thus, the aging progression with highest to lowest values is PVDF-GL > PP-GS > PVDF-GS. The change in surficial properties can be further explained by the introduction of oxygen functional groups during electrochemical aging which made all the BPPs more hydrophilic (Figure 7 (a)). Though, the change in surface roughness (Figure 7 (b)) was hard to distinguish, most likely due to surface inhomogeneity of the BPPs causing high standard deviation. But the surface roughness changes could be owed to slight material abrasion or moderate gas evolution occurring at the BPP surface during CV cycling in the vanadium electrolyte.

Thus from above it can be inferred that the surfacial properties siginificantly influence the electrochemcial behaviour/stability of each BPP.

To validate the findings of the electrochemical experiments and to evaluate the electrochemical behaviour of the BPPs, single cell VRFB tests with each composite BPP were performed. Various factors, such as vanadium ion precipitation, resistance change of membrane, felt electrode and electrolyte as well as change in electrode polarization might

actively contribute to a VRFB performance decline, but they are difficult to define and distinguish from each other (17). Thus, this characterization is beyond the scope of this publication. However, since the single cell test parameters were the same for the measurements with only the type of BPP being changed, it is presumed that any change in the evaluated VRFB performance was related to the applied BPP. The 1st and 200th charge/discharge curves from each VRFB test were plotted and compared (Figure 8). In the initial cycle all three cells show the typical charge/discharge behaviour of a VRFB. The VRFB cell containing PP-GS exhibits the lowest capacity and reaches the cut off voltage earliest probably due to its lower electrical conductivity compared to the other both BPPs. Whereas the VRFB with PVDF-GL had better charge/discharge behaviour during the 1st cycle compared to PVDF-GS and PP-GS probably because of its high electrical conductivity. However, due to its low electrochemical stability, its VRFB performance significantly deteriorated, which is in good agreement with the electrochemical CV test results.

The efficiencies and state of health from the single cell experiments were plotted in **Fehler! Verweisquelle konnte nicht gefunden werden.**. In general, the voltage efficiency is influenced by the activation overpotential, ohmic resistances (17, 18) and the electrolyte crossover (17, 18). It is assumed that the voltage efficiency is mainly affected by the exchange of the three different types of BPPs since all other components and their influence on the ohmic resistance remain unchanged within the single cell battery. [7]. As observed from the evaluated charge/discharge curves, the poor PVDF-GL VRFB voltage efficiency (Figure 9 (a)) could be due to low electrochemical stability caused by poor surficial properties, as explained under the electrochemical CV measurement discussion, leading to the high ohmic resistance. Initially, the VRFB with the PP-GS had higher voltage efficiency compared to that with PVDF-GS, presumably due to its lower surface roughness which might have reduced the contact resistance. But owed to the relatively poorer electrochemical stability as charge-discharge cycles progressed its performance eventually declined.

The coulombic efficiency in a VRFB is generally influenced by mass transport losses and vanadium ion crossover through the membrane (19, 20). In addition, it also provides information about faradic losses caused by possible side reactions (17). As can be seen in Figure 9 (b) the coulombic efficiencies of the cells, containing PP-GS and PVDF-GS are

comparable. The decreased coulombic efficiency of the PVDF-GL VRFB can be attributed to side reactions such as continuous oxidation of the graphite surface as indicated by the rising $Q_{Q/HQ}$ activity quantified in the electrochemical CV measurements.

The energy efficiency is the product of the coulombic and voltage efficiency. The performance of the VRFBs with the PVDF-GS and PP-GS have a similar efficiency but the latter gradually declines slightly more than PVDF-GS after 120 cycles. In general, PVDF-GL provides the lowest efficiency (Figure 9 (c)). The electrochemical aging and analysis of the BPPs show the same trend.

As the cycling progresses the SoH declines for all VRFB tests, most likely because of vanadium ion crossover and side reactions causing a difference in the state-of-charge between the two half-cell electrolytes and aging of the battery components (Figure 9 (d)) Moreover, the continuous increase of the cell resistance would decrease the rate capability and the capacity that can be discharged at the given current density. The lowest electrochemical stability of PVDF-GL leads to higher drop of SoH, whereas the VRFB cells with BPPs containing smaller graphite PS, show less SoH decline.

Conclusions

The composition of each individual BPP influences its surficial, electrical and electrochemical behaviour. The PVDF-GL with large average graphite PS (75 µm) exhibits higher surface roughness and higher accessible porosity compared to composites with smaller graphite PS i.e. PP-GS (25 µm) and PVDF-GS (25 µm). The electrical properties of the examined BPPs were influenced by the polymer type. The electrochemical aging of each BPP was asserted through quantification of C_{dl}, $Q_{Q/HQ}$ and $Q_{V^{4+}/V^{5+}}$. The PVDF-GL had the lowest electrochemical stability compared to PP-GS and PVDF-GS owing to its higher hydrophilicity, surface roughness and accessible porosity. Thus, these surficial properties have a significant influence on the electrochemical behaviour. The influence of the BPPs on the single cell VRFB performance was evaluated by $\eta_{V,C,E}$, and SoH. A similar trend was observed in electrochemical aging and analysis, i.e., PVDF-GL showed the worst performance followed by PP-GS and PVDF-GS which is in good agreement with the single cell evaluation.

Hence, a good electrochemical stability of the BPPs is essential in order to reduce side reactions and to obtain a long BPP and electrolyte cycle life for battery operation. The proposed potentiodynamic electrochemical characterization method can help to determine the electrochemical stability of BPPs by identification and quantification of the aging features. Also, it can be an effective foresight to predict the applicability of a BPP in a VRFB.

Acknowledgments

The authors are thankful to the German Federal Ministry of Economic Affairs and Energy for funding the project “Top Level Redox Flow” Grant Agreement Number ZF4090701ZG5.

References

1. Caglar B, Conductive Polymer Composites And Coated Metals As Alternative Bipolar Plate Materials For All-Vanadium Redox-Flow Batteries. Advanced Materials Letters. 2014;5(6):299-308.

2. Ghimire PC, Bhattarai A, Schweiss R, Scherer GG, Wai N, Lim TM, Investigation of Reactant Conversion in the Vanadium Redox Flow Battery Using Spatially Resolved State of Charge Mapping. Batteries. 2019;5(1):2.

3. Barton JL, Brushett FR. A One-Dimensional Stack Model for Redox Flow Battery Analysis and Operation. Batteries. 2019;5(1).

4. Satola B, Kirchner CN, Komsiyska L, Wittstock G, Chemical Stability of Graphite-Polypropylene Bipolar Plates for the Vanadium Redox Flow Battery at Resting State. Journal of The Electrochemical Society. 2016;163(10):A2318-A25.

5. Jung M, Lee W, Nambi Krishnan N, Kim S, Gupta G, Komsiyska L, Harms C, Kwon Y, Henkensmeier D, Porous-Nafion/PBI composite membranes and Nafion/PBI blend membranes for vanadium redox flow batteries. Applied Surface Science. 2018;450:301-11.

6. Liu H, Yang L, Xu Q, Yan C, Corrosion behavior of a bipolar plate of carbon–polythene composite in a vanadium redox flow battery. RSC Advances. 2015;5(8):5928-32.

7. Lim JW, Lee DG, Carbon fiber/polyethylene bipolar plate-carbon felt electrode assembly for vanadium redox flow batteries (VRFB). Composite Structures. 2015;134:483-92.

8. Park M, Jung Y-J, Ryu J, Cho J. Material selection and optimization for highly stable composite bipolar plates in vanadium redox flow batteries. J Mater Chem A. 2014;2(38):15808-15.

9. Caglar B, Richards J, Fischer P, Tuebke J. Conductive polymer composites and coated metals as alternative bipolar plate materials for all-vanadium redox-flow batteries. Adv Mat Lett. 2017;5(6):10.

10. Zhang J, Zhou T, Xia L, Yuan C, Zhang W, Zhang A. Polypropylene elastomer composite for the all-vanadium redox flow battery: current collector materials. Journal of Materials Chemistry A. 2015;3(5):2387-98.

11. Lee NJ, Lee S-W, Kim K, Kim J-H, Park M-S, Jeong G, Kim Y-J, Byun D, Development of Carbon Composite Bipolar Plates for Vanadium Redox Flow Batteries. Bull Korean Chem Soc. 2012;33(11):3589-92.

12. Satola B, Komsiyska L, Wittstock G, Bulk Aging of Graphite-Polypropylene Current Collectors Induced by Electrochemical Cycling in the Positive Electrolyte of Vanadium Redox Flow Batteries. Journal of The Electrochemical Society. 2017;164(12):A2566-A72.

13. Hammer E-M, Berger B, Komsiyska L, Improvement of the Performance of Graphite Felt Electrodes for Vanadium-Redox-Flow-Batteries by Plasma Treatment. Int Journal of Renewable Energy Development. 2014;3(1):6.

14. Ebnesajjad S, 2 - Fluoropolymers: Properties and Structure. In: Ebnesajjad S, editor. Melt Processible Fluoroplastics. Norwich, NY: William Andrew Publishing; 2003. p. 9-21.

15. Selke SE, Hernandez RJ, Packaging: Polymers in Flexible Packaging. In: Buschow KHJ, Cahn RW, Flemings MC, Ilschner B, Kramer EJ, Mahajan S, Veyssière P, editors. Encyclopedia of Materials: Science and Technology. Oxford: Elsevier; 2001. p. 6652-6.

16. Chmiola J, Yushin G, Dash RK, Hoffman EN, Fischer JE, Barsoum MW, Gogotsi Y, Double-Layer Capacitance of Carbide Derived Carbons in Sulfuric Acid. Electrochem Solid State Lett. 2005;8(7):A357.

17. Park S-K, Shim J, Yang JH, Jin C-S, Lee BS, Lee Y-S, Shin K-H, Jeon J-D, The influence of compressed carbon felt electrodes on the performance of a vanadium redox flow battery. Electrochimica Acta. 2014;116:447-52.

18. Yang L, Thou Y, Wang S, Lin Y, Huang T, Yu a. A Novel Bipolar Plate Design Vanadium Redox Flow Battery Application. Int J Electrochem Sci. 2017;12:8.
19. Kim S. Vanadium Redox Flow Batteries: Electrochemical Engineering. In: Demirkan MT, Attita A, editors. Energy Storage Devices2019. p. 20.
20. Ashraf Gandomi Y, Aaron DS, Mench MM. Coupled Membrane Transport Parameters for Ionic Species in All-Vanadium Redox Flow Batteries. Electrochim Acta. 2016;218:174-90.

Tables

Table 1: Investigated graphite-polymer composite BPPs

BPP	**Constituents wt. [%]**			
	PP	**PVDF**	**GS**	**GL**
PP-GS	14		86	-
PVDF-GS	-	20	80	-
PVDF-GL	-	20	-	80

Table 2: Structural properties of the composite BPPs and the PS of the raw graphite particles used in production of the BPPs

Properties / **BPP**	**Average graphite PS in raw graphite powders [µm]**	**Accessible-porosity [%]**	S_q **[µm]**	**Density [g cm^{-3}]**
PP-GS	25	2.7	0.45 ± 0.2	1.8
PVDF-GS	25	2.4	0.73 ± 0.4	2.1
PVDF-GL	75	3.1	0.99 ± 0.3	2.1

Figure Captions

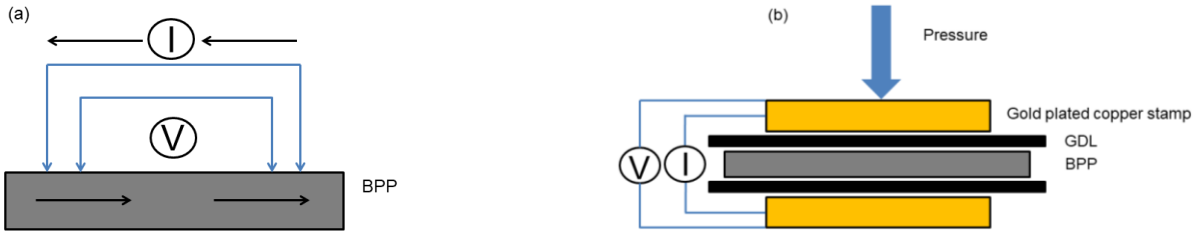

Figure 1: (a) In-plane and (b) through-plane electrical conductivity measurement setup for BPPs

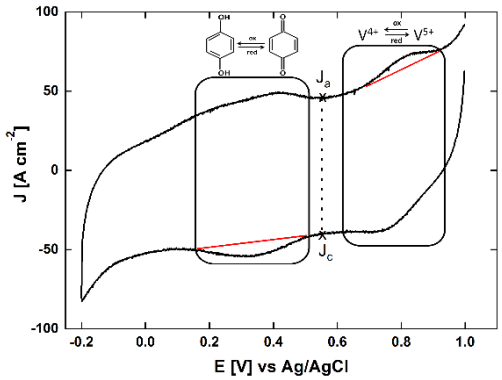

$$C_{dl} = \frac{(J_a - J_c)}{2 \times \frac{dE}{dt}} \; [mF\ cm^{-2}]$$

$$Q_{Q/HQ}\,,\, Q_{V^{4+}/V^{5+}} = \frac{\int_{E_1}^{E_2} J \times dE}{\frac{dE}{dt}} \; [\mu C\ cm^{-2}]$$

$$where \frac{dE}{dt} : scan\ rate$$

Figure 2: Example and determination of electrochemical aging features of the BPP in 0.1 M H_2SO_4 solution (red line indicates the integration of the curve done on originlab software)

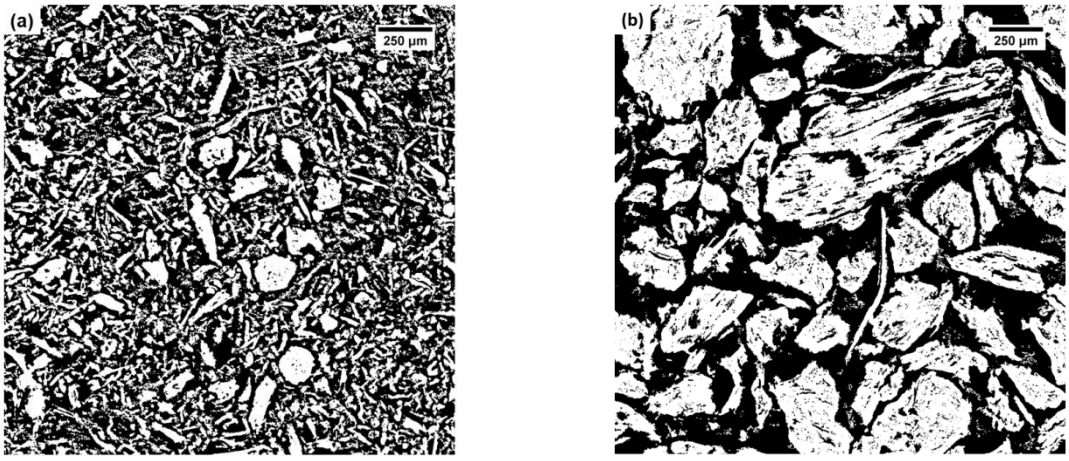

Figure 3: mCT 2D images of a) GS and b) GL graphite powders at 1 µm/pixel resolution

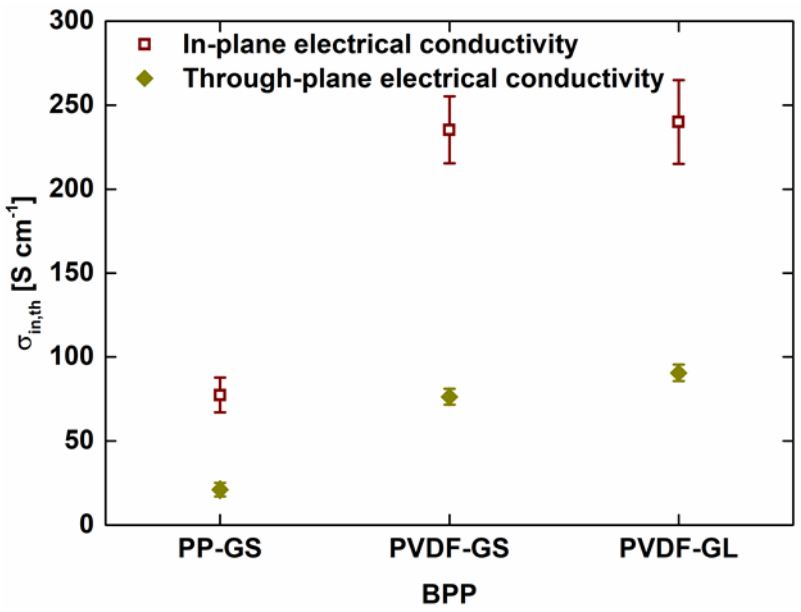

Figure 4: In-plane and through-plane electrical conductivity of pristine composite BPPs

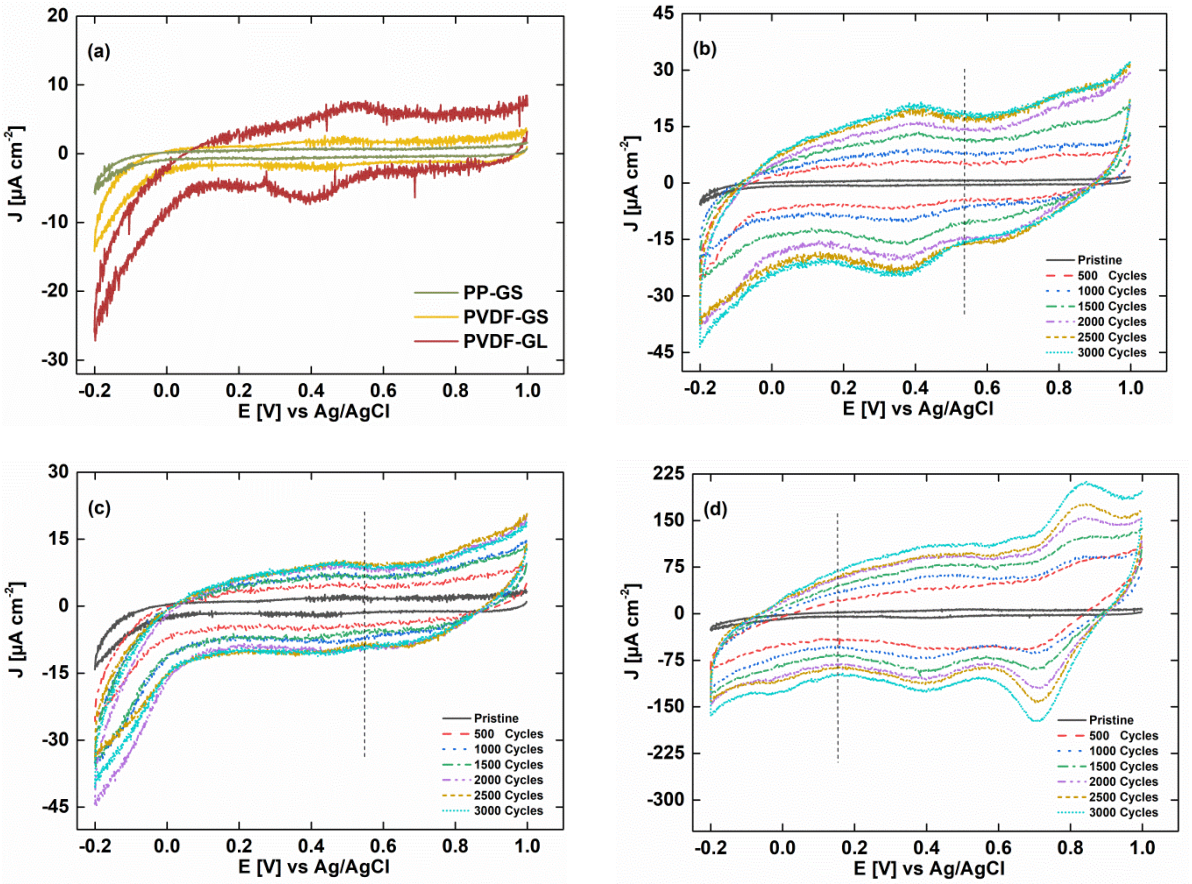

Figure 5: Comparing CV curves from BPPs in 0.1 M H_2SO_4 solution at a scan rate of 5 mV s^{-1}. (a) Pre-aged BPPs and (b) PP-GS, (c) PVDF-GS and (d) PVDF-GL BPPs pristine and after aging.

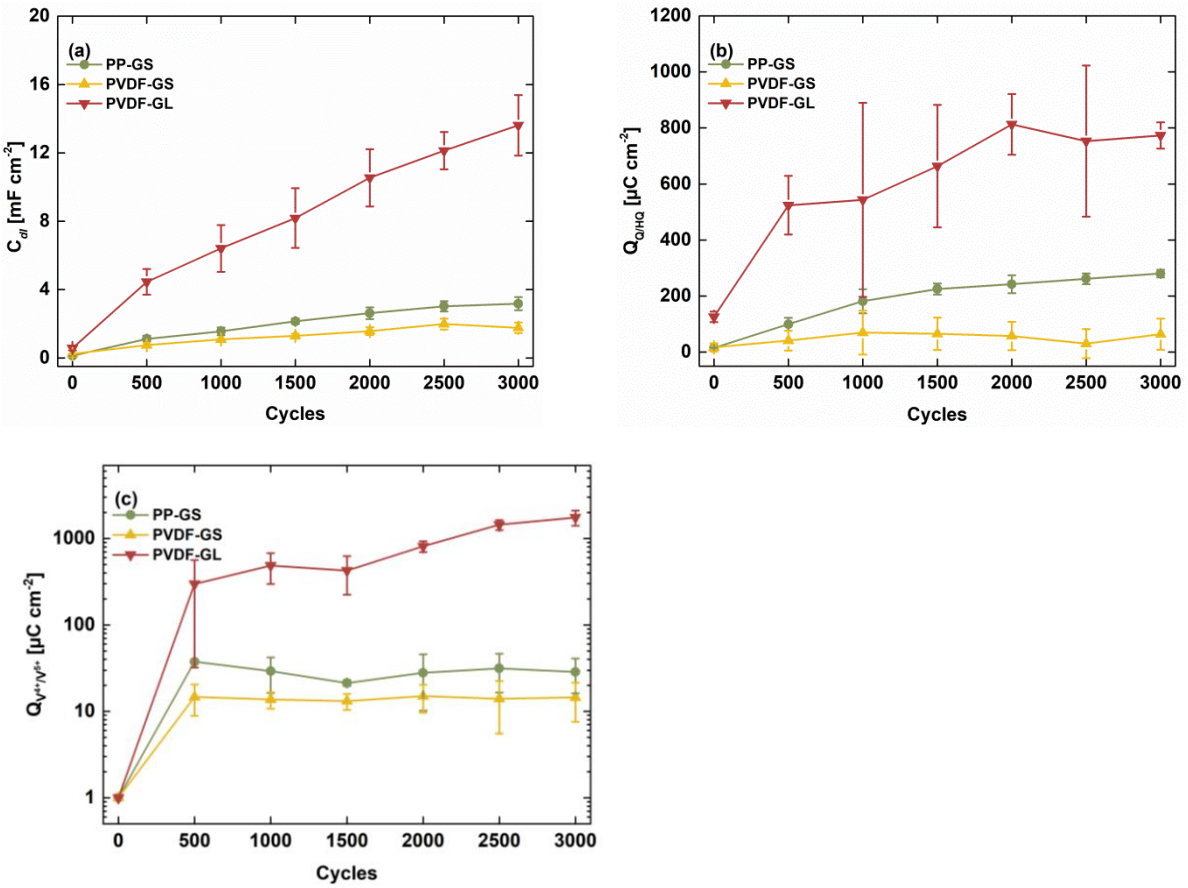

Figure 6: (a) Double layer capacitance, (b) quinone/hydroquinone activity and (c) vanadium redox activity in 0.1 M H_2SO_4 solution of each composite BPP after aging in vanadium electrolyte.

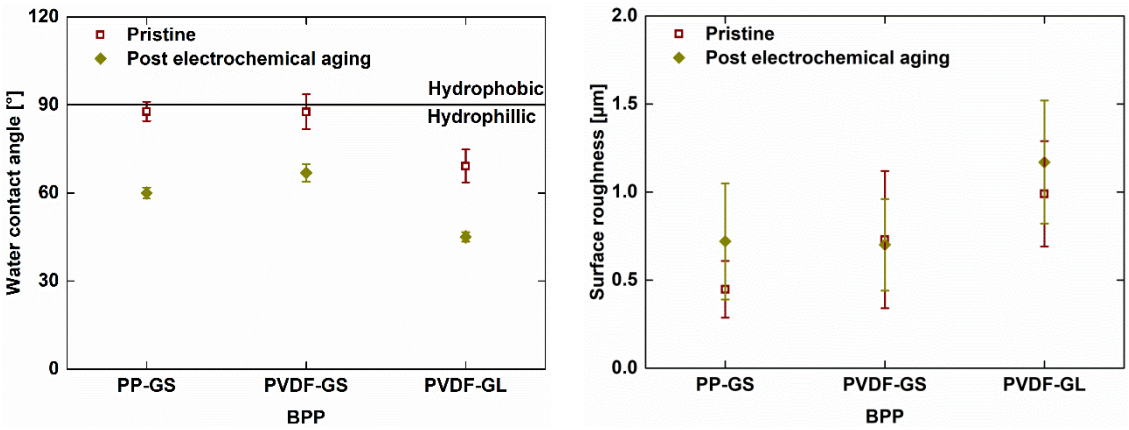

Figure 7: (a) Water contact angle and (b) surface roughness of pristine and electrochemically aged composite BPPs after 3000 CV cycles in vanadium electrolyte

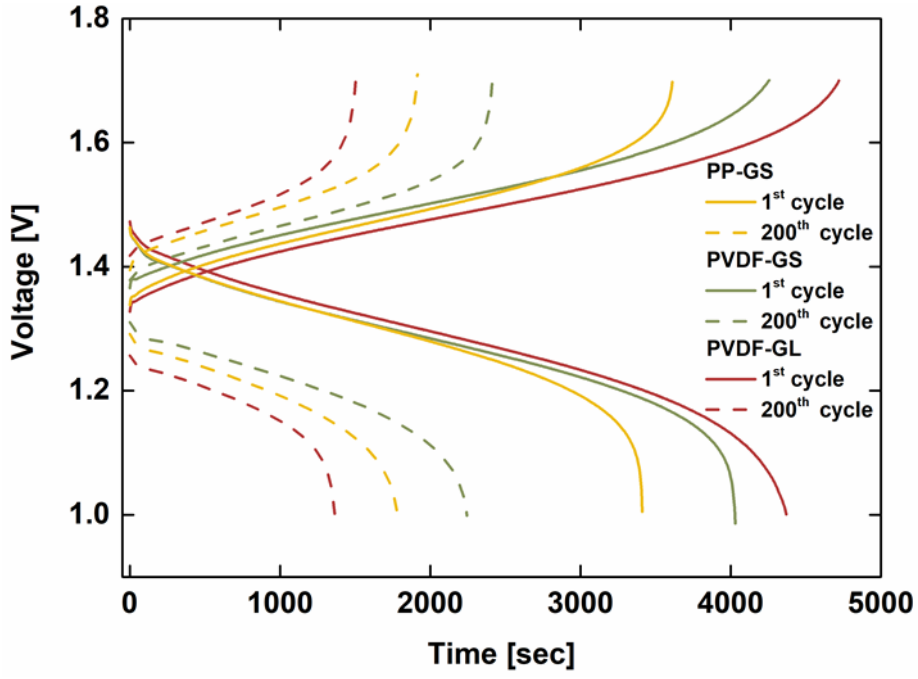

Figure 8: Comparison of charge/discharge cycles of VRFB single cell tests with each BPP at current density of 60 mA cm^{-2}